Shifting hail hazard under global warming

Timothy H. Raupach[1,2,3*], Raphael Portmann[4,5], Christian Siderius[6], Steven C. Sherwood[2,3]

[1]Institute for Climate Risk and Response, UNSW Sydney, Mathews Building Level 4, The University of New South Wales, Sydney, 2051, NSW, Australia.
[2]Climate Change Research Centre, UNSW Sydney, Australia.
[3]ARC Centre of Excellence for Climate Extremes, UNSW Sydney, Australia.
[4]Agroscope, Swiss Federal Office for Agriculture, Zurich, Switzerland (prev. address).
[5]Planval, Bern, Switzerland.
[6]Uncharted Waters Research, Sydney, Australia.

*Corresponding author(s). E-mail(s): timothy.h.raupach@gmail.com;

Abstract

Hailstorms cause significant damage across the globe, but changes to hailstorms in a warming climate are not well quantified. Here, we applied hail proxies to global model projections to quantify changes in the frequency of hail-prone conditions and the effects of those changes on 26 crop types. In projections with 2 °C and 3 °C of mean global warming, hail-prone conditions shift poleward, with decreases in hail frequency across the mid-latitudes and increases in colder regions. In general, hail-prone frequency is projected to decrease in summer and increase in winter, leading to projected increases in the hail-prone proportion of cropping season for winter crops and decreases for summer crops.

Keywords: hail, severe weather, convection, trends, projections

Hailstorms are a form of extreme weather that causes significant damage to physical assets including crops. Hail and the storms that produce it are expected to be affected by anthropogenic global warming, yet regional studies using observations or projections show geographical inhomogeneities and there remains high uncertainty on the

details of any changes [1–3]. Globally, hail observations are scarce [3], meaning global climatologies generally rely on satellite data [4, 5] or examination of environmental conditions in reanalyses using hail proxies [6]. Here, we produced global projections of future hail hazard using hail proxies applied to model output from the Coupled Model Intercomparison Project (CMIP6) [7] in a per-degree framework, and used them to analyse projected changes in hail frequency and resulting changes in hail risk to crops.

Because hailstorms are hard to observe and model given their small spatial size and relative rarity [3], proxies that detect hail-prone atmospheric conditions are often used in climatological studies. Hail proxies rely on detecting the atmospheric "ingredients" required for hail to form. Hailstones form by accretion of supercooled liquid water onto ice embryos suspended in the updraft of a thunderstorm, until they become too heavy to support, after which they fall while melting on their descent through warmer air [8, 9]. Hailstorm ingredients are usually considered to include, at a minimum, atmospheric instability, for a thunderstorm with strong updrafts that can support hail growth to form [10], and vertical wind shear (differences in horizontal wind by height) to "organise" the storm [11] and influence hailstone trajectories [12, 13]. Instability–shear hail proxies are common [14]. Proxies suffer from the "initiation problem", in that storms rarely initiate even in storm-prone conditions [14–16].

Climate change is expected to affect the ingredients for hailstorms and thus the frequency and severity of hailstorms themselves [3]. A thermodynamic expectation is of three offsetting effects: first, increased instability owing to a larger saturation deficit in a warmer atmosphere [17] leading to more storm initiation and stronger updrafts that could support larger hailstones; second, increased melting of hailstones owing to a warmer troposphere [18], thus leading to a reduction (or elimination [19]) of surface hail frequency; and third, an overall decrease in vertical wind shear [11] that is often outweighed by changes in instability [20, 21] or may not apply locally [22, 23]. The broad thermodynamic expectation is thus of a reduction in surface hail frequency combined with an increase in severity when hail does reach the Earth's surface [3]. However, regional studies show large geographical heterogeneity in signals for hail frequency, owing in part to offsetting in these climate change effects and in part to dynamical changes meaning that ingredient changes are not spatially uniform, while hail severity is generally expected to increase [3].

Here, we applied four hail proxies to an ensemble of eight global projections from CMIP6, to examine future projections of the frequency of hail-prone conditions globally. We investigated the effects of projected changes on hail-prone proportions of crop growing seasons for 26 different crops. We used a per-degree framework [24] for simpler comparisons between models. For details of the simulations and proxies used, refer to "Online methods" and the supplementary information. Our work shows that, generally, hailstorm frequency is projected to decrease in warmer environments but increase in cooler environments in future, driven primarily by changes in convective instability. A sensitivity analysis shows that the projected changes would increase hail occurrence risk to current winter crops, while decreasing occurrence risk for summer crops.

Results

Comparison to ERA5 for the historical period

Figure 1 shows a comparison between the multimodel, multi-proxy mean of annual hail-prone days for the CMIP6 models, and the multi-proxy mean of annual hail-prone days for the ERA5 reanalysis, for 1980–1999. While individual CMIP6 models produced a wide range of absolute values of hail-prone days (Supplementary Figure 1), the locations of hail hotspots agreed well between reanalysis and models. The models MPI-ESM1-2-HR and EC-Earth produced similar numbers of hail-prone days to ERA5, while MIROC6, CMCC-CM2-SR5, and CMCC-ESM2 showed moderately more and CNRM-CM6-1 and GISS-E2-1-G showed significantly more hail-prone days than ERA5. There were also differences across the selected hail proxies, with the Significant Hail Parameter (SHIP) [25] producing the fewest, and the modified proxy of Raupach et al., 2023 [14] without extra conditions (RaupachNEC) producing the greatest number of hail-prone days, respectively. Different proxies highlighted similar geographical regions but differed in magnitudes of hail-prone days. Given the models produced geographical agreement but differences in absolute numbers of hail-prone days, we focus on changes in multi-proxy, multimodel means in the rest of our analyses.

Case studies of hail-prone day anomalies

Monthly multi-proxy mean anomalies in hail-prone days derived using ERA5 reanalysis showed higher values for months with known occurrences of damaging hailstorms. The proxies produced higher than climatological average numbers of hail-prone days for February and March 2015 in northern and central India (Supplementary Figure 2), regions that were affected by hailstorms that caused major losses to wheat crops in this period [26, 27]. Similarly, the proxies highlighted areas of central and southern Europe as particularly hail-prone in June 2022 (Supplementary Figure 3), when the passage of two low-pressure systems caused hailstorm outbreaks across these regions [28] that broke records for insured losses in France [29]. The proxies also identified April 2015 and October 2022 as unusually hail-prone months in northeast India and western France, respectively; there were hailstorms reported in both regions during these respective months [26, 28]. These case-study results increase our confidence in the ability of the multi-proxy mean to identify hail-prone conditions worldwide, despite the individual proxies having been trained using data from Australia [14], Italy [30], and the United States [25].

Changes in hail-prone days with warming

Figure 2 shows multimodel, multi-proxy mean changes in annual hail-prone days for 2 °C and 3 °C of global warming, respectively. These changes are shown as relative differences zoomed to selected land areas in Figures 3 and 4. Changes are similar between the two epochs, with a general increase in the change magnitude in the 3 °C scenario. Changes generally agreed across the Raupach proxies and SHIP, while the pure instability–shear proxy of Eccel [30] produced contrasting increases across the tropics (Supplementary Figures 4 and 5). The mean changes show an overall poleward shift

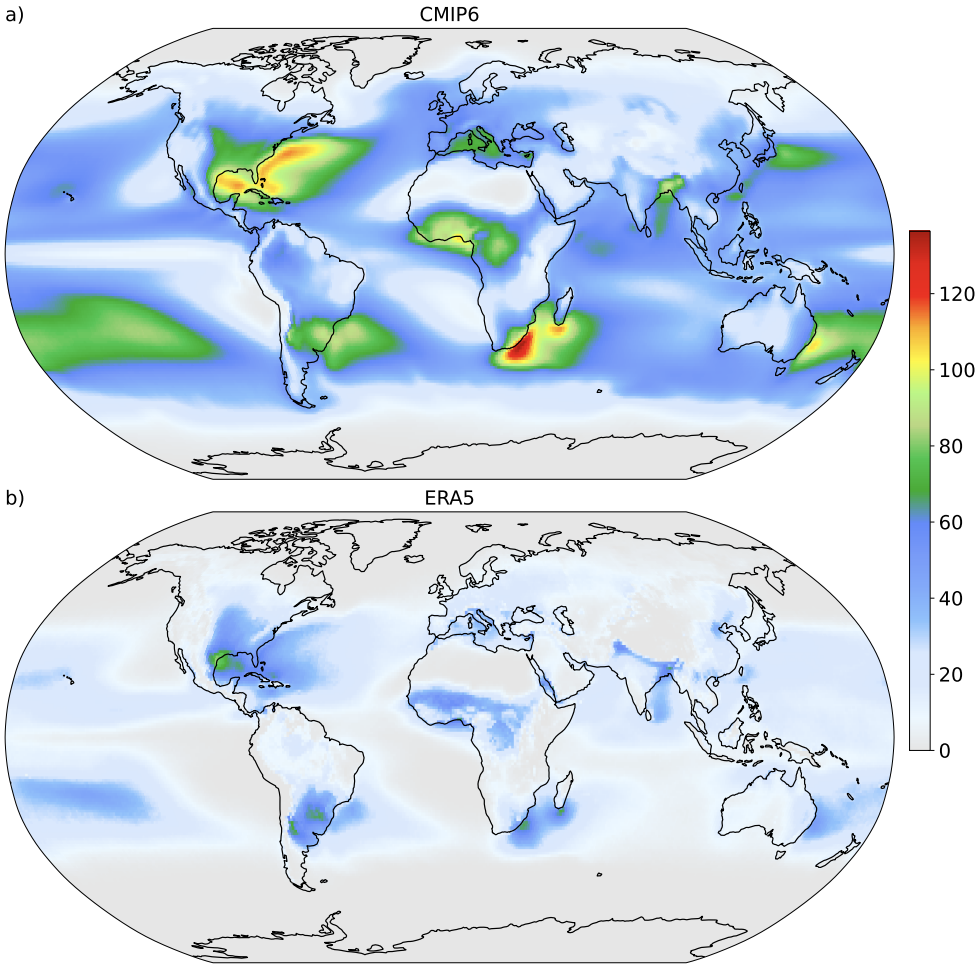

Fig. 1 Hail proxies show known hail-prone regions in both projections and reanalysis. Multimodel, multi-proxy mean annual hail-prone days for CMIP6 models (a), and multi-proxy mean annual hail-prone days for ERA5 reanalysis (b), for four selected proxies over the historical period (1980-1999) at 1 × 1 ° resolution.

of hail-prone conditions under both warming scenarios, with increases in hail-prone condition frequency projected across land areas in central-north Asia, New Zealand's south island, Tasmania and the southeast of Australia, North America north of about 50° N, South America in the southern Pampas and west to the Andes, Europe north of about 60° N and in the vicinity of the Alps and southeast of the Black Sea, North Africa over the eastern part of the Sahara, and a very small region in eastern South Africa. Decreases in hail-prone day frequency were projected in southeast coastal areas of India and China, connecting in a band across mainland Southeast Asia, northern Australia, the southeast United States and Mexico, the northern region of South America and east of the Andes between about 10° S and 30° S, the North Atlantic

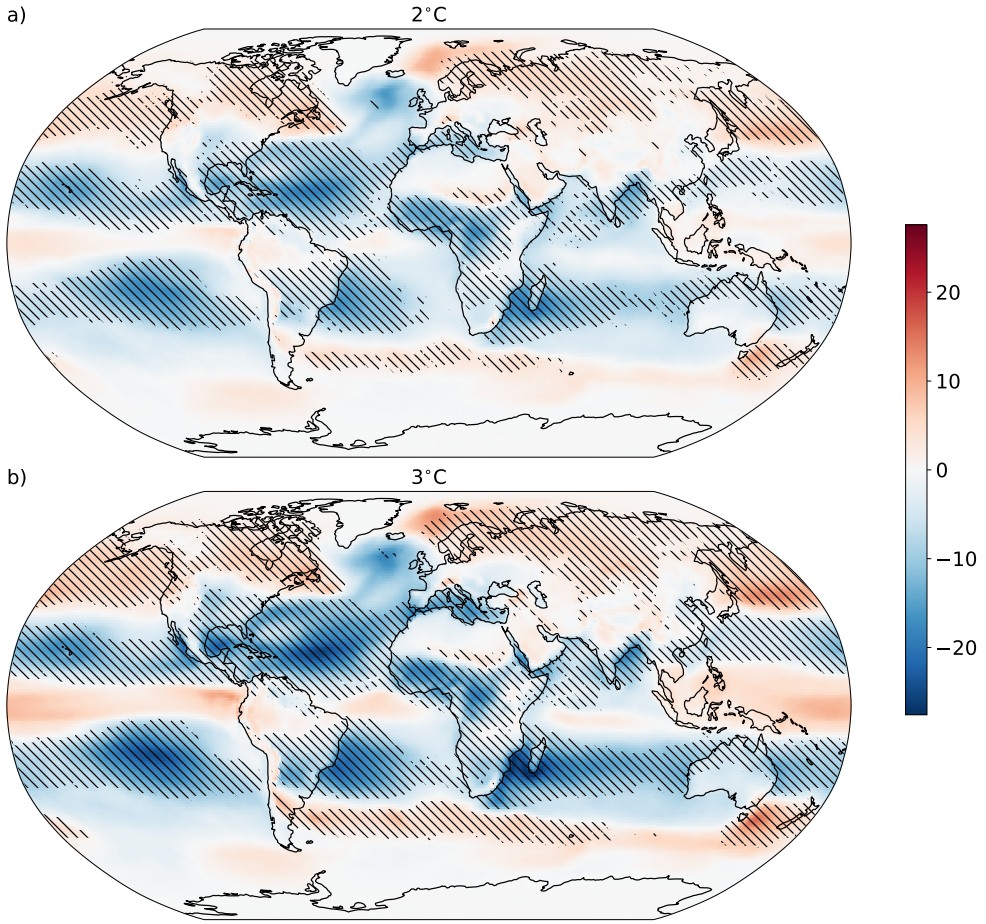

Fig. 2 Hail-prone conditions shift under warming projections. Multi-proxy, multimodel mean changes in annual hail-prone days for 2 °C (a) and 3 °C (b) of global warming. Stippling shows regions in which at least 50% of the model/proxy combinations agreed with the sign of the mean difference and also showed significant differences in the mean ($p < 0.05$ on a t-test on two related samples).

and Mediterranean coasts of Africa, and most of Africa south of 15° N. Seasonal analyses showed that the increases are concentrated in the cold season and decreases in the warm season (Supplementary Figure 6).

Projected changes in proxy ingredients

Future projections of storm-relevant properties showed almost uniform increases in convective instability, with increases in extreme values of convective available potential energy (CAPE) and lifted index (LI), and increasing convective inhibition that may lead to more explosive development of severe storms (Supplementary Figure 7). Projections in extremes in 0-6 km bulk wind shear (S06) showed decreases (mixed increases)

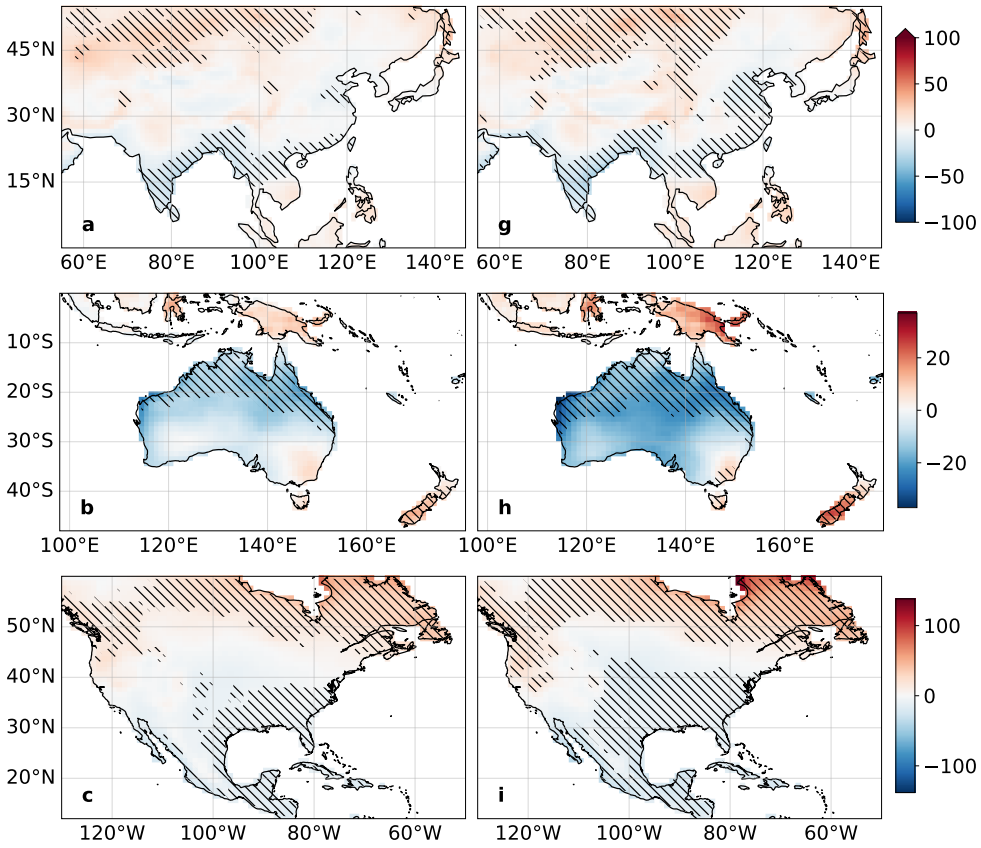

Fig. 3 Multi-proxy, multimodel mean changes in annual hail-prone days by region. Changes are shown as a percentage of multi-proxy, multimodel mean historical hail-prone days over land, for 2 °C warming (a-c) and 3 °C warming (g-i) for Asia (a, g), Australasia (b, h), and North America (c, i). Stippling as for Figure 2. Colour bars are shared across rows; to increase contrast the colour bar for a and g is truncated.

in the northern (southern) hemisphere (Supplementary Figure 7). Temperature-related ingredients increased as expected in the warmer scenarios (Supplementary Figure 8).

Changes in hail-prone proportions of cropping periods

Figure 5 shows changes in the proportion of crop growing time that is considered hail-prone, for 26 crops by world region. For the historic period, the African tropics showed particularly high proportions of hail-prone cropping periods for millet, sorghum, soybeans, maize, groundnuts/peanuts, and pulses (Supplementary Figure 9). Warming of 2 °C and 3 °C was projected to reduce the hail-prone cropping period for these crops while increasing the risk for crops grown in more poleward regions (Supplementary Figures 10 and 11).

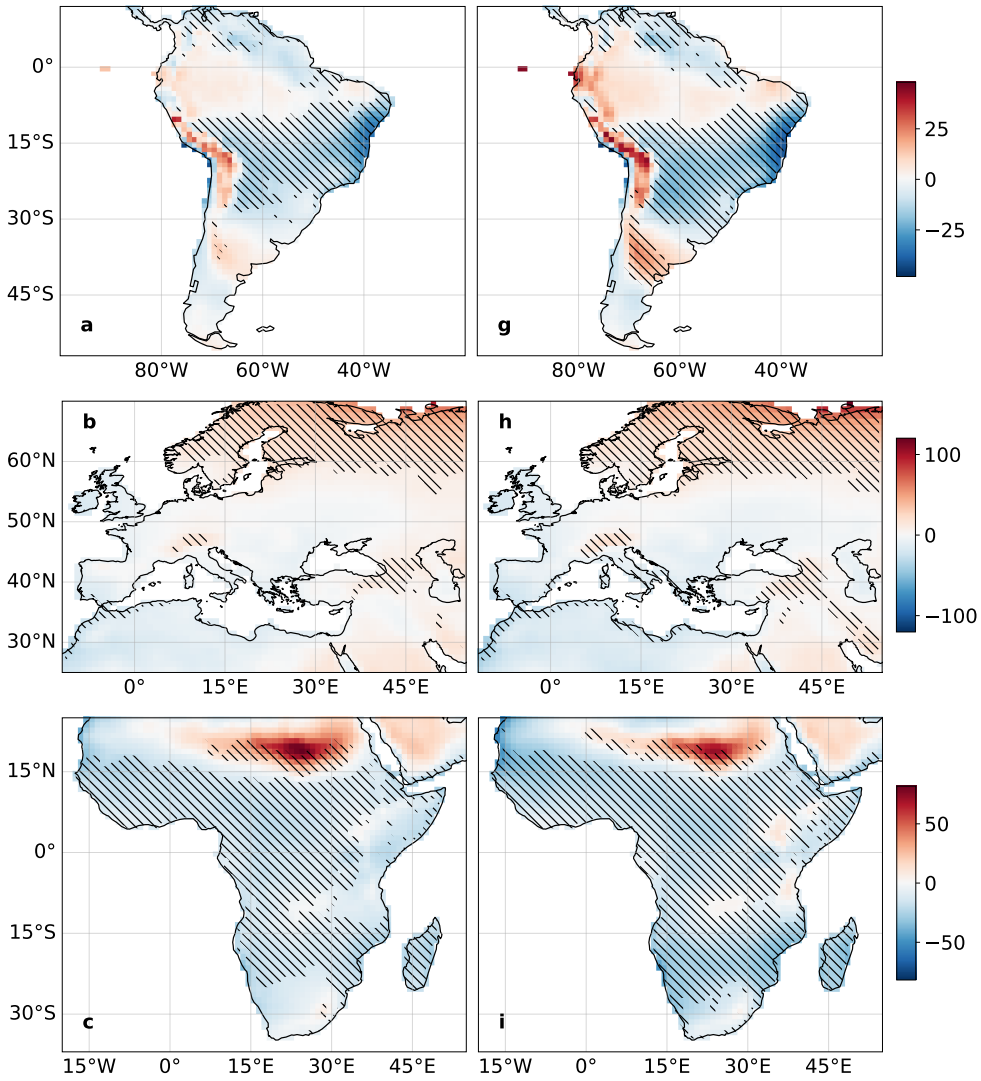

Fig. 4 As for Figure 3 but for South America (a, g), Europe (b, h), and Africa (c, i).

In Africa, all crops were projected to experience fewer hail-prone days, with regional increases not statistically significant (Supplementary Figure 12). In Asia, (Supplementary Figure 13), there were a variety of responses, with decreasing hail-prone cropping periods in India and generally in China. Increases in the hail-prone proportion of cropping seasons were projected particularly across the north for barley, fodder grasses, grapes/vine, rapeseed/canola, rye, and wheat. Maize was projected to experience a greater hail-prone proportion of the cropping season in southeastern china but a lesser proportion in the northeast, while wheat and rapeseed/canola showed strong increases in hail-prone cropping season proportion in northeastern China.

In Europe, most non-significant changes were decreases, but significant changes indicated increases in hail-prone cropping season proportion for barley, fodder grasses, grapes/vine, maize, potatoes, pulses, rapeseed/canola, rye, wheat, and other annual and perennial crops. The significant increases were generally concentrated in a zonal band at around 60°N and in regions around the Alps in Western Europe, an area to the southeast of the Black Sea, and in southern Iran (Supplementary Figure 14). Increases in hail-prone cropping proportion for rye were heavily concentrated in Finland, Estonia, Latvia, and the adjoining areas of Russia. In North America, there were significant increases for barley and rye in particular, with regional increases in the hail-prone proportion for these crops across the central and eastern USA. For other crops, there were generally decreases in hail-prone cropping season proportion projected in the southeast, with increases projected in the northeast and across northern Canada (Supplementary Figure 15). In Oceania, barley was projected to have increased hail-prone cropping season proportion, albeit with a large range in projected changes, while all other crops showed projected decreases in hail risk. Significant decreases were concentrated in Australia's northeast, while significant increases were concentrated in a small region of southeast Australia and the South Island of New Zealand (Supplementary Figure 16). In South America, all crops show projected decreased risk, but there are possible increases for barley, millet, and rye in the 3 °C scenario. Regional changes show statistically significant increases in hail hazard for several crops, for example maize and potatoes, in a region of the southern Pampas and west to the Andes (Supplementary Figure 17).

Examinations of monthly changes for point locations (Supplementary Figures 18 and 19) highlight that the crops with the greatest increases in risk are those with winter cropping periods, while those with the greatest reductions in risk are those that grow across summer periods. **(Include two case study locations as a way of circling back. Chris writes: "There is no agreement on India (Fig 3a) but a hint of hail-prone days increasing. Southern France shows agreement and increase, at least in the area adjacent to the Alps (4a). Re India, better check the wheat and rice cropping periods. MIRCA has split these crops evenly among the two main seasons in northern India - the two main crops, which is wrong (I might have mentioned before). Wheat growing season should (only) be from Nov-Apr in Punjab, Uttar Pradesh and Haryana. Harvest starts in March but in many regions extends into April, especially when winter has been colder than usual and the crop takes longer to grow. I can imagine this would expose a much higher fraction to hail risk. Rice is grown primarily from Jul-Oct.")**

Drivers of the projected changes

Figure 6 shows the main drivers of projected changes in this study, shown as the difference between projected changes and changes when the future values for single ingredients were de-biased. The ingredients driving the changes depended on the proxy. Overall, increases in hail-prone environment frequency were driven by instability increases, while reductions in hail-prone environment frequency were driven by temperature-related ingredients. The sums of changes across de-biased ingredients

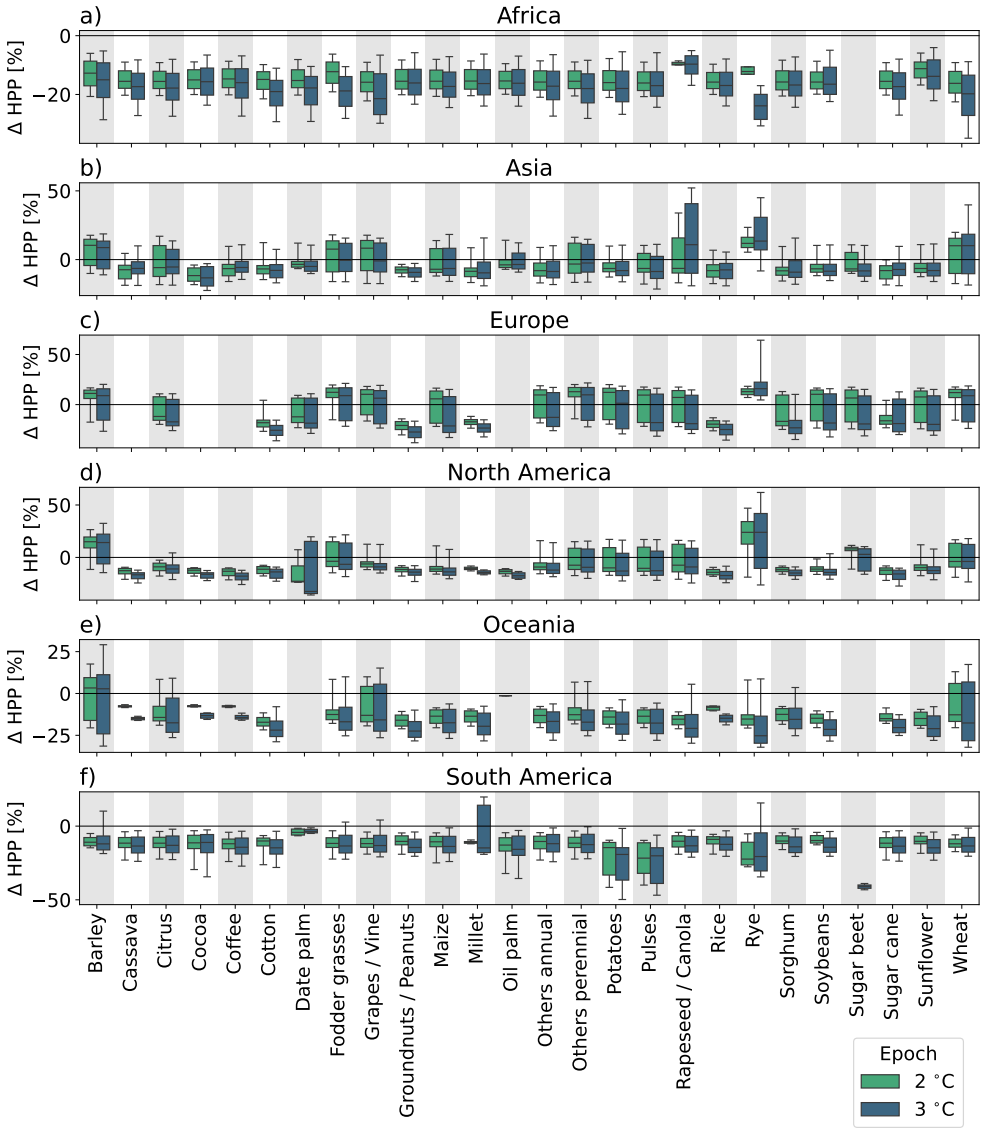

Fig. 5 Distributions of significant changes in hail-prone crop proportion (HPP) by crop, epoch, and world region. Regions are defined as in Figure 3. Changes are multimodel, multi-proxy mean changes in hail-prone crop proportion, shown as a percentage of the multimodel, multi-proxy mean historical hail-prone crop proportion. Significant changes are those for which at least 50% of the model/proxy combinations agreed with the sign of the mean difference and also showed significant differences in the mean ($p < 0.05$ using Welch's t-test). Coloured boxes show interquartile ranges, whiskers show 10th-90th percentile ranges.

were close to the projected changes where no ingredients were de-biased, indicating that these results explain most of the projected changes, with the small differences that remain likely related to interactions between ingredients. The large differences

between the Eccel proxy and the other proxies were caused by the instability–shear proxy reacting to increases in instability without explicitly accounting for temperature changes. Changes in SHIP were driven mainly by changes in the most-unstable mixing ratio. In the Raupach proxies, increases in hail-prone days owing to instability increases are offset by changes in melting level height and T_{500}.

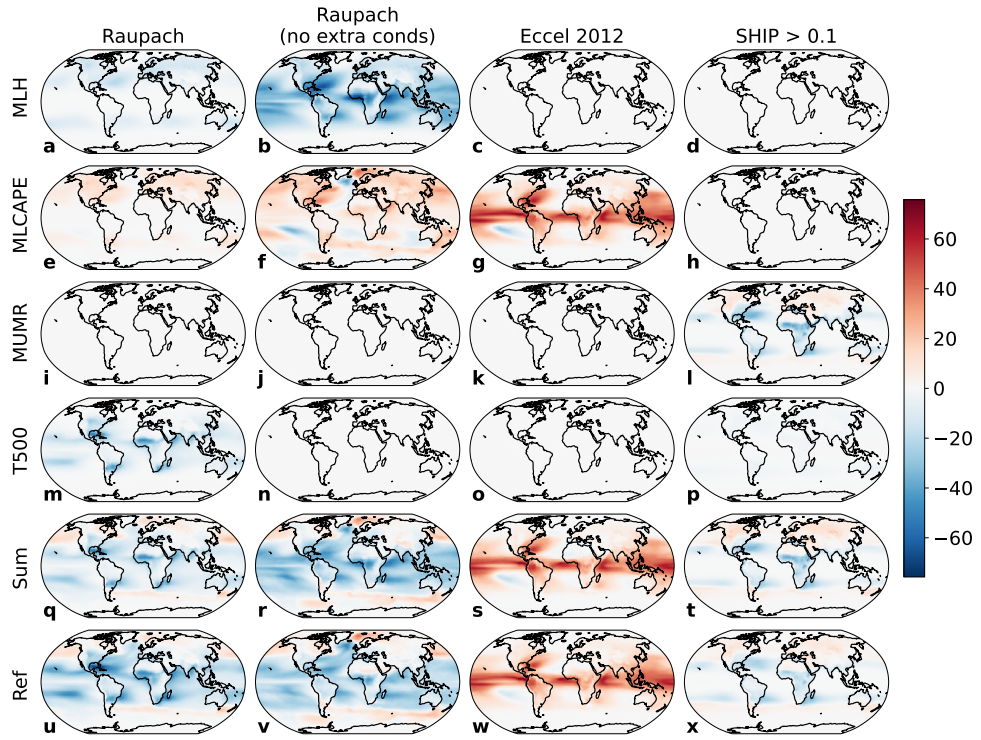

Fig. 6 The main drivers of the projected changes (all drivers are shown in Supplementary Figure 20). All plots are multimodel means. Plots show the difference in hail prone days between historical and the 3C epoch for unchanged ingredients, minus the difference with the given ingredient de-biased in the 3C epoch. Red (blue) areas show where an ingredient added to (subtracted from) the projected change. Ingredients shown here are melting level height (MLH, a-d), mixed-layer CAPE (MLCAPE, e-h), most-unstable mixing ratio (MUMR, i-l), and temperature at 500 hPa (T500, m-p). "Sum" (q-t) shows sums across changes from all de-biased ingredients (column sums from Supplementary Figure 20) and "Ref" (u-x) shows the projected changes per proxy when no ingredients were de-biased. Columns show hail proxies and the colour scale is in annual hail days.

Discussion

- Although we show proxy results globally, the proxies used were trained using land-based reports [14, 30] and there is uncertainty in the occurrence of hail in maritime storms [8].

- Proxies trained in one region cannot be assumed to be perfectly applicable globally since storm properties differ by location **(Taszarek, Brooks)**. However, the Raupach proxies are specifically designed to take spatial variability in storm conditions into account by using the melting level height, and have been shown to perform reasonably across the Australian continent which contains a wide variety of storm environments [31], and the multi-proxy means are shown in Section **(ref)** to be able to identify particularly hail-prone conditions in areas in which the proxies used here were not trained. Further, we use **(relative?)** differences **(by model?)**.
- Leung et al., 2023 also observed a northward shift in hailstorms in the US from 2000 (preprint at https://assets.researchsquare.com/files/rs-3217821/v1_covered_a256d1b8-b2e0-41b6-ab9c-e2628059bc91.pdf?c=1699615569.)
- It is clear that Eccel 2012 shows an increase where the Raupach proxies and SHIP show decreases. This is explained by the non-Eccel proxies taking changes in temperature explicitly into account, but the discrepancy also increases the uncertainty in these results.
- **(Chris writes: "Re discussion: A limitation to the approach - which we discussed before - is that we are not shifting the cropping periods or expand/relocate growing areas in future as this would get too complicated/is hard to quantify. To pre-empt any questions, could we mention that the poleward shift in hail risk is similar to the shift in suitable growing areas as identified in studies x and y, so fraction exposed might not change drastically or at least not reduce? Or would that be waking up sleeping dogs..?")**
- **(Raphael writes: Regarding the crops: yes, I was thinking of the same. Or one could just take the last 4 months before harvest.Its a bit challenging because the duration of the different cropping phases might vary quite a bit across regions. I found this map where for each month and global region the vegetative phase is indicated for the most important crops that might give some indication: https://ipad.fas.usda.gov/ogamaps/cropmapsandcalendars.aspx when you go to December -¿ Europe ¿ you see: winter wheat: dormant, which means it is not growing. If you then go to April it changes to: vegetative. And thats when it starts to get relevant for hail. actually, there is a publication for this work: https://cdnsciencepub.com/doi/full/10.1139/cjps-2020-0231?af=R")**
- Fits with hailstone "dichotomy" reported for the USA by [32] and it is likely that severe hail will have different trends than "all hail" shown here.

Online methods

Data

A filtering approach was used to select models from the Coupled Model Intercomparison Project Phase 6 (CMIP6) [7]. We selected models that contained variables required to calculate convective indices: air temperature at the surface (`tas`) and by model level (`ta`), wind vectors at the surface (`uas` and `vas`) and by level (`ua` and `va`),

specific humidity at the surface (`huss`) and by level (`hus`), and surface pressure (`ps`). We filtered for models with a temporal resolution at least as fine as six-hourly (those with "table IDs" of `3hr` or `6hrLev`), and models that were available for both historical and SSP5-8.5 experiments ("experiment IDs" of `historical` or `ssp585`). Further, the models had to be available in the National Computational Infrastructure (NCI) node of the Earth System Grid Federation (ESGF), and had to cover the required epochs. The resulting CMIP6 models, that we used here, are detailed in Supplementary Table 1. If model orography was available in the `orog` variable, it was used; if not, the orography of the historical runs of CNRM-CM6-1 (ensemble r1i1p1f2) was interpolated onto the model grid and used instead [33]. Reanalyses were European Centre for Medium-range Weather Forecasts (ECMWF) reanalysis 5 (ERA5) data [34] on pressure levels [35]. To match the CMIP6 model characteristics, we used global ERA5 data at 00, 06, 12, and 18 UTC for each day from 1980 to 1999, interpolated to $1° \times 1°$ resolution.

Calculation of convective parameters

Convective parameters were calculated as described for the proxy of Raupach et al., 2023 [14], for each CMIP6 dataset at its native resolution and for downscaled ERA5 data. For each CMIP6 model, annual and seasonal statistics were calculated, then all statistics were interpolated onto a $1° \times 1°$ grid for comparison.

Application of hail proxies

We applied four hail-specific instability-shear proxies to CMIP6 and ERA5 data: Raupach, RaupachNEC, Eccel, and SHIP. The proxies were, respectively, a modified version of the proxy in Raupach et al., 2023 with (Raupach) and without (RaupachNEC) "extra conditions" to remove false positives [14], that of Eccel et al., 2012 [30], and a threshold of 0.1 on the Significant Hail Parameter (SHIP) [25]. The modifications made Raupach and RaupachNEC are detailed in Supplementary Material Section 2. Other proxies were tested but excluded from this study. The proxies of Kunz 2007 [36] and Mohr and Kunz, 2013 [37] produced unrealistically many hail-prone days in tropical regions for which they were not trained [14], and a threshold of 0.5 on SHIP, as has been used in other studies for severe hail [6], was found to produce too few hail-prone days in comparison with the other proxies designed for hail of any size (Supplementary Figure 21).

Per-degree framework

The historical period used for each model was 1980–1999. The epochs that represented 2 °C and 3 °C warming compared to the historical period were determined per model using 20-year running means of monthly global average temperature anomalies (Supplementary Figure 22).

Calculation of drivers

For each hail proxy ingredient, de-biased versions of the 3 °C epoch were calculated using `python-cmethods` v2.3.0 [38] using the quantile-mapping method with 100 quantiles and the historical period as the baseline.

Data availability. MIRCA2000 data are available with identifier https://doi.org/10.5281/zenodo.7422506.

Code availability. Convective indices were calculated using `xarray_parcel` by T. H. Raupach (https://doi.org/10.5281/zenodo.8088497) **(Update version with new xarray release)**. Warming levels were calculated using code by T. H. Raupach **(ref)**.

Acknowledgements. This research was undertaken with the assistance of resources and services from the NCI, which is supported by the Australian Government. THR acknowledges financial support from QBE Insurance.

Competing interests. Since March 2024 THR's position at UNSW Sydney has been financially supported by QBE Insurance. The authors declare no other competing financial or non-financial interests.

Author contributions.

References

[1] Allen, J. T. *Climate Change and Severe Thunderstorms*, 67 (Oxford Univ. Press, 2018). URL https://oxfordre.com/climatescience/view/10.1093/acrefore/9780190228620.001.0001/acrefore-9780190228620-e-62.

[2] Brimelow, J. *Hail and Hailstorms*, 58 (Oxford Univ. Press, 2018). URL https://oxfordre.com/climatescience/view/10.1093/acrefore/9780190228620.001.0001/acrefore-9780190228620-e-666.

[3] Raupach, T. H. *et al.* The effects of climate change on hailstorms. *Nat. Rev. Earth Environ.* **2**, 213–226 (2021).

[4] Cecil, D. J. & Blankenship, C. B. Toward a global climatology of severe hailstorms as estimated by satellite passive microwave imagers. *J. Climate* **25**, 687–703 (2012).

[5] Bang, S. D. & Cecil, D. J. Constructing a multifrequency passive microwave hail retrieval and climatology in the GPM domain. *J. Appl. Meteorol.* **58**, 1889–1904 (2019).

[6] Prein, A. F. & Holland, G. J. Global estimates of damaging hail hazard. *Weather Clim. Extremes* **22**, 10–23 (2018).

[7] Eyring, V. *et al.* Overview of the Coupled Model Intercomparison Project Phase 6 (CMIP6) experimental design and organization. *Geosci. Model Dev.* **9**, 1937–1958 (2016).

[8] Knight, C. A. & Knight, N. C. in *Hailstorms* (ed.Doswell, C. A.) *Severe Convective Storms* 223–254 (American Meteorological Society, Boston, MA, 2001).

[9] Fraile, R., Castro, A., López, L., Sánchez, J. L. & Palencia, C. The influence of melting on hailstone size distribution. *Atmos. Res.* **67-68**, 203–213 (2003).

[10] Brooks, H. E., Lee, J. W. & Craven, J. P. The spatial distribution of severe thunderstorm and tornado environments from global reanalysis data. *Atmos. Res.* **67-68**, 73–94 (2003). European Conference on Severe Storms 2002.

[11] Brooks, H. E. Severe thunderstorms and climate change. *Atmos. Res.* **123**, 129–138 (2013).

[12] Dennis, E. J. & Kumjian, M. R. The impact of vertical wind shear on hail growth in simulated supercells. *J. Atmos. Sci.* **74**, 641–663 (2017).

[13] Lin, Y. & Kumjian, M. R. Influences of CAPE on hail production in simulated supercell storms. *J. Atmos. Sci.* **79**, 179–204 (2022).

[14] Raupach, T. H., Soderholm, J., Protat, A. & Sherwood, S. C. An improved instability–shear hail proxy for australia. *Mon. Weather Rev.* **151**, 545–567 (2023).

[15] Sherwood, S. C. Convective precursors and predictability in the tropical western Pacific. *Mon. Weather Rev.* **127**, 2977–2991 (1999).

[16] Tippett, M. K., Allen, J. T., Gensini, V. A. & Brooks, H. E. Climate and hazardous convective weather. *Curr. Clim. Change Rep.* **1**, 60–73 (2015).

[17] Seeley, J. T. & Romps, D. M. Why does tropical convective available potential energy (CAPE) increase with warming? *Geophys. Res. Lett.* **42**, 10,429–10,437 (2015).

[18] Prein, A. F. & Heymsfield, A. J. Increased melting level height impacts surface precipitation phase and intensity. *Nat. Clim. Change* **10**, 771–776 (2020).

[19] Mahoney, K., Alexander, M. A., Thompson, G., Barsugli, J. J. & Scott, J. D. Changes in hail and flood risk in high-resolution simulations over Colorado's mountains. *Nat. Clim. Change* **2**, 125–131 (2012).

[20] Trapp, R. J., Diffenbaugh, N. S. & Gluhovsky, A. Transient response of severe thunderstorm forcing to elevated greenhouse gas concentrations. *Geophys. Res. Lett.* **36**, L01703 (2009).

[21] Allen, J. T., Karoly, D. J. & Walsh, K. J. Future Australian severe thunderstorm environments. Part II: The influence of a strongly warming climate on convective environments. *J. Climate* **27**, 3848–3868 (2014).

[22] Diffenbaugh, N. S., Scherer, M. & Trapp, R. J. Robust increases in severe thunderstorm environments in response to greenhouse forcing. *P. Natl. Acad. Sci. USA* **110**, 16361–16366 (2013).

[23] Rädler, A. T., Groenemeijer, P. H., Faust, E., Sausen, R. & Púčik, T. Frequency of severe thunderstorms across Europe expected to increase in the 21st century due to rising instability. *npj Clim. Atmos. Sci.* **2**, 30 (2019).

[24] Lepore, C., Abernathey, R., Henderson, N., Allen, J. T. & Tippett, M. K. Future global convective environments in CMIP6 models. *Earth's Future* **9**, e2021EF002277 (2021).

[25] NOAA SPC. Significant hail parameter. https://www.spc.noaa.gov/exper/mesoanalysis/help/help_sigh.html (2022). National Oceanographic and Atmospheric Administration National Weather Service Storm Prediction Center, accessed 21 June 2022.

[26] Chattopadhyay, N., Devi, S. S., John, G. & Choudhari, V. Occurrence of hail storms and strategies to minimize its effect on crops. *Mausam* **68**, 75–92 (2017).

[27] Singh, S. K., Saxena, R., Porwal, A., Ray, N. & Ray, S. S. Assessment of hailstorm damage in wheat crop using remote sensing. *Curr Sci India* **112**, 2095–2100 (2017).

[28] Pucik, T. Major hailstorms of 2022 (2023). URL https://www.essl.org/cms/major-hailstorms-of-2022/. Accessed 2024-01-10.

[29] Soyka, T. Severe 2022 hail damage in france sets new benchmarks, underscores shift of risk and calls for pricing adjustments (2023). URL https://www.swissre.com/risk-knowledge/mitigating-climate-risk/hail-damage-risk-france-2022.html. Accessed 2024-01-10.

[30] Eccel, E., Cau, P., Riemann-Campe, K. & Biasioli, F. Quantitative hail monitoring in an alpine area: 35-year climatology and links with atmospheric variables. *Int. J. Climatol.* **3**, 503–517 (2012).

[31] Raupach, T. H., Soderholm, J. S., Warren, R. A. & Sherwood, S. C. Changes in hail hazard across australia: 1979-2021. *npj Clim. Atmos. Sci.* **6**, 143 (2023).

[32] Gensini, V. A. *et al.* Hailstone size dichotomy in a warming climate. *npj Clim. Atmos. Sci.* **7**, 185 (2024).

[33] Bracegirdle, T. J. *et al.* Twenty first century changes in Antarctic and Southern Ocean surface climate in CMIP6. *Atmos. Sci. Lett.* **21**, e984 (2020).

[34] Hersbach, H. *et al.* The ERA5 global reanalysis. *Q. J. Roy. Meteor. Soc.* **146**, 1999–2049 (2020).

[35] Hersbach, H. *et al.* ERA5 hourly data on pressure levels from 1979 to present (2018). Copernicus Climate Change Service (C3S) Climate Data Store (CDS).

[36] Kunz, M. The skill of convective parameters and indices to predict isolated and severe thunderstorms. *Nat. Hazards Earth Sys.* **7**, 327–342 (2007).

[37] Mohr, S. & Kunz, M. Recent trends and variabilities of convective parameters relevant for hail events in Germany and Europe. *Atmos. Res.* **123**, 211–228 (2013).

[38] Schwertfeger, B. T. btschwertfeger/python-cmethods: v2.3.0 (2024). URL https://doi.org/10.5281/zenodo.12168002.